Journal of Applied Fluid Mechanics, Vol. 9, No. 2, pp. 839-853, 2016.
Available online at www.jafmonline.net, ISSN 1735-3572, EISSN 1735-3645.
DOI: 10.18869/acadpub.jafm.68.225.24454

Hysteresis and Shear Velocity in Unsteady Flows

G. Bombar

Ege University, Dept. of Civil Eng., İzmir, 35100, Turkey

Corresponding Author Email: gokcen.bombar@ege.edu.tr

(Received January 5, 2015; accepted March 28, 2015)

ABSTRACT

The shear velocity is an important parameter in characterizing the shear at the boundary in open channels and there exist methods to estimate the shear velocity in steady flows, but the application and comparison of these methods to non-uniform unsteady flows is limited. In this study, three artificial triangular-shaped hydrographs were generated where the base flow is non-uniform with fine sand bed and the shear velocity was obtained by the methods, u_{*SV} by using the Saint-Venant equations, u_{*L} by using the procedure given by Clauser Method, u_{*P} by using the parabolic law, u_{*UN} by using the momentum equation assuming the slope of energy grade line is equal to bed slope and u_{*avg} by using the average velocity equation are used in this study. The stream-wise components of velocity time series and the velocity profiles were obtained by means of an acoustic Doppler velocity meter. The variation of the shear velocity and the constant for the parabolic law with time is discussed. It is concluded that the shear velocities found by the parabolic law and the average velocity equation can be used interchangeably. Furthermore a hysteresis intensity parameter is proposed in order to examine the depth variation of hysteretic behavior of depth variation both with point velocity and average velocity. It is revealed that the more the unsteady the hydrograph the more the hysteresis both in terms of point velocity and cross-sectional mean velocity.

Keywords: Unsteady flow; Shear velocity; Hysteresis; Velocity time series; Parabolic law; Clauser method; Saint-Venant Equations.

NOMENCLATURE

A	cross sectional area
B	channel width
B_r	integral constant for rough boundaries
B_s	integral constant for smooth boundaries
Cu	uniformity coefficient
d_{10}	particle size at which 10% is finer
d_{50}	median diameter of the sediment
d_{65}	particle size at which 65% is finer
d_{84}	particle size at which 84% is finer
d_g	geometric mean diameter was
F_{base}	Froude number at base flow conditions
F_{peak}	Froude number at peak flow conditions
g	gravitational acceleration
h	flow depth
h_{base}	base flow depth
h_{peak},	peak flow depth
H_{PSCU}	speed of pump in % of 1450 rpm
k_s	equivalent sand roughness
q_{base}	unit discharge at base flow conditions
q_{peak}	unit discharge at peak flow conditions
Q	flow rate
Q_{base}	discharge at base flow conditions
$Q_{FM\ peak}$	peak discharge from flow meter
Q_{FM}	discharge from flow meter
Q_{peak},	discharge at peak flow conditions
Q_{VM}	discharge from velocity measurements
$Q_{VM\ peak}$	peak discharge from velocity
$u_{avg\ smt}$	smoothed average
u_{avg}.	velocity by averaging the repetitions
u_m	maximum velocity,
u_*	shear (friction) velocity
u_{*avg}	u_* obtained by Eq. (14)
u_{*L}	u_* estimated by Clauser Method
u_{*P}	u_* estimated by the Parabolic Law
u_{*SV}	u_* estimated by Saint-Venant equation
u_{*UN}	u_* obtained by Eq. (3)
u_z	mean point velocity at z
u_m	maximum velocity
V	average flow velocity
V_{base}	base flow velocity
V_c	$(V_{base}+V_{peak})/2$
V_{peak},	peak flow velocity
w	instantaneous point velocity in z dir.
w'	fluctuating components in z dir.
$\overline{w}$	time varying mean point velocity in z dir.
x	axis for stream-wise direction
z	axis for vertical direction
z_0	reference level
α	dimensionless unsteadiness parameter
χ	limit between inner and outer layers
σ_g	geometric standard deviation
ν	kinematic viscosity

R^2	correlation coefficients.
R_h	hydraulic radius
S_0	channel slope
S_e	slope of the energy grade line
T_f	falling duration based on the flow depth
T_{fQ}	falling duration based on the flow rate
T_r	rising duration based on the flow depth
T_{rQ}	rising duration based on the flow rate
$T_{r\ QFM}$	rising duration based on Q_{FM}
$T_{r\ QVM}$	rising duration based on Q_{VM}
T_{rV}	rising duration based on the velocity
u	instantaneous point velocity in x dir.
u'	fluctuating components in x dir.
$\overline{u}$	time varying mean point velocity in x dir
κ	von Karman constant
λ	constant in parabolic law
η	hysteresis intensity parameter
τ	shear stress
τ_0	boundary shear stress
ρ	density of the water
Π	wake strength parameter
Δh	h_{peak} - h_{base}
ΔQ_{FM}	$Q_{FM\ peak}$ - $Q_{FM\ base}$,
ΔQ_{VM}	$Q_{VM\ peak}$ - $Q_{VM\ base}$,
ΔT	T_r + T_f
ΔV	V_{peak} - V_{base}
$\forall_{FM}$	total volume of water considering Q_{FM}
$\forall_{VM}$	total volume of water considering Q_{VM}
$\omega(\Pi)$	wake function

1. INTRODUCTION

Velocity distribution and flow parameters such as turbulence and boundary shear stress in steady flow conditions were studied widely both experimentally in laboratory and in the field (Nezu and Rodi 1986, Cardoso *et al.* 1989, Kırkgöz 1989, Kırkgöz and Ardıçlıoğlu 1997, Kabiri-Samani *et al.* 2013, Genç *et al.* (2015)) and numerically (Song *et al.* 2012, Debnath *et al.* 2015, Shah *et al.* 2015). However, in nature, unsteady flows are the most common type of open channel flows and attracted a great amount of interest for research in the field of hydraulics (Bose and Dey 2012) particularly in the furrow irrigation and in irrigation management systems (Walker and Humpherys 1983, Meselhe and Holly 1993, Kumar *et al*. 2002, Zhang *et al*. 2012).

The experiments in open channels were conducted on hydraulically rough surfaces by Tu (1991), Song and Graf (1996), Qu (2002) and Bares *et al*. (2008) and on smooth surfaces by Nezu *et al*. (1997). Tu (1991) and Qu (2002) used micro-mouline; Nezu *et al*. (1997) used Laser Doppler Anemometer (LDA) for point velocity measurement at various elevations on the flow depth by repeating the experiment at various times to obtain the velocity profile. Song and Graf (1996) and later Bagherimiyab (2012) used Acoustic Doppler Velocity Profiler (ADVP) (Lhermitte and Lemmin 1994) which uses ultrasonic method to obtain the velocity profile once in each sampling time. Qu (2002) worked on both fixed and mobile beds. During the rising and falling limbs of the hydrograph, the validity of logarithmic law distribution has been investigated (Nezu and Sanjou 2006). The flow features like average velocity, turbulence intensity, Reynolds stress and shear velocity (Nezu *et al*. 1997, Song 1994, Tu 1991, Bares *et al*. 2008) are the issues investigated in unsteady flow conditions which were carried out in the laboratory studies.

In order to represent the intensity of the hydrograph which can be defined as the change of flow depth or flow rate within a specified time interval, the unsteadiness parameter is used (Nezu *et al.* 1997). There exist many parameters defining unsteadiness proposed by many researchers (Nezu *et al.* 1997; Rowinski *et al.* 2000, Bombar *et al.* 2011, Bombar 2014) such as α;

$$\alpha = (1/V_c)/(\Delta h/T_{rQ}) \tag{1}$$

where $\Delta h=h_{peak}-h_{base}$, h_{base} and h_{peak}, are the base flow depth and peak flow depths, $V_c=(V_{base}+V_{peak})/2$, V_{base} and V_{peak}, are the base flow and peak flow average velocities, T_{rQ} is the rising duration of the hydrograph based on the flow rate as depicted in Fig. 1. Here t is time, Q is the flow rate, Q_{base} and Q_{peak}, are the base discharge and peak discharge, T_{fQ} is the falling duration of the hydrograph based on the flow rate, $\Delta Q=Q_{peak}-Q_{base}$, h is the flow depth T_r and T_f are the rising and falling durations of the hydrograph based on the flow depth and , $\Delta T= T_r + T_f$.

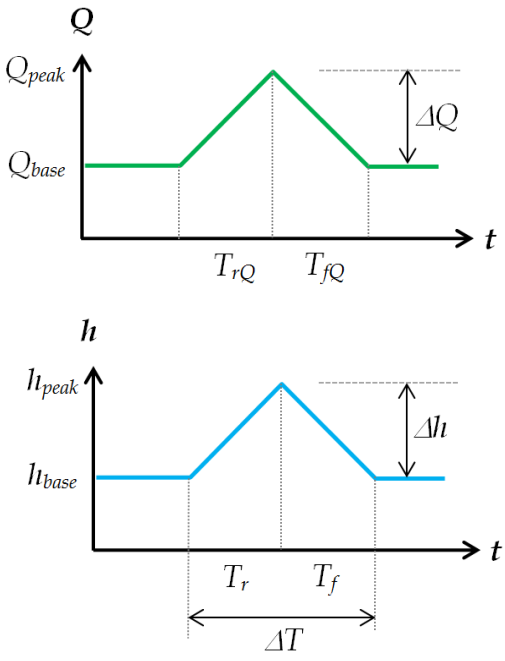

Fig. 1. Representation of the terms of a hydrograph in terms of time variation of flow rate and flow depth.

In unsteady flows it is a well-known fact that there exists a hysteresis between flow depth and mean cross sectional velocity where the velocity reaches its maximum value before the flow depth (Graf and Altınakar 1998, Nezu and Sanjou 2006). The mean velocity attains its maximum value before flow depth does (Nezu and Nakagawa 1991, Qu 2002). Song and Graf (1996), Bares *et al*. (2008), find out that the shear velocity attains its maximum value first and then in the order of *V*, *Q* and finally *h*. Qu (2002) observed that the limbs of the curve becomes farther as the unsteadiness increases. Jensen *et al.* (1989) investigated this time lag too (Nezu and Sanjou 2006).

According to Nezu (2005) and Nezu and Nakagawa (1993), in steady flows the shear velocity can be calculated in many ways (Lopez and Garcia 1999, Muste and Patel 1997), such as, the use of Reynolds stress graph, velocity data at the viscous sub-layer, Clauser method, parabolic law, the slope method where Saint-Venant equations are used and average velocity equation. Under unsteady flow conditions, some researchers prefer to estimate the shear stress using the depth-slope product rule corresponding to normal (steady, uniform) flow especially when the purpose of their study is to focus on overall parameters rather than local parameters (Hassan *et al*. 2006, Güney *et al*. 2013) or prefer to neglect the contribution of velocity gradient to energy slope (Powell *et al*. 2001). Qu (2002), Song and Graf (1996) and Afzalimehr *et al*. (2007) used some of these methods in unsteady flows, but the comparison of these methods is limited.

This study was carried out in the laboratory with artificial triangular-shaped hydrographs with high unsteadiness at which the base flow is non-uniform. Among the methods that have been developed to estimate the shear velocity (u_*), u_{*SV} the Saint-Venant equations, u_{*L} the procedure given by Clauser Method, u_{*P} the parabolic law and u_{*UN} the momentum equation assuming the slope of energy grade line is equal to bed slope and the equation for average velocity u_{*avg} are used which are explained below. Furthermore the hysteresis was investigated and a hysteresis intensity parameter is proposed in order to find out the depth variation of hysteretic behavior at point velocity and average velocity.

2. THEORETICAL REVIEW

The related methods are explained as follows.

1. Reynolds Stress Graph:

In uniform flows the total shear stress τ varies linearly with depth as given in Eq. (2) having the value of τ_0 at the boundary and zero at the free surface. By linear extrapolation of the Reynolds stress profile, the shear velocity can be calculated knowing that $u_* = (\tau_0/\rho)^{0.5}$.

$$\tau = -\rho\overline{u'w'} + \rho\nu\,\partial u/\partial z = \rho u_*^2\left(1 - z/h\right) \qquad (2)$$

where ρ is density, u' and w' fluctuating components in stream-wise direction x and vertical direction z, ν is the kinematic viscosity, u is the stream-wise component of velocity.

This method requires a high sampling frequency. In accelerating non-uniform flows the type of the graph is convex and decelerating flows it has a concave type. Muste and Patel (1997) used this method in calculating the shear velocity (or friction velocity) for flows with suspended sediment. In unsteady flow conditions, this method was used by Song and Graf (1996).

2. The slope method, Saint-Venant Equations (u_{*UN} & u_{*SV}):

In steady uniform flows, from momentum balance u_* is related to gravitational acceleration g, channel slope S_0 and R_h as

$$u_* = \sqrt{gR_hS_0} \qquad (3)$$

As the shear velocity varies around the wetted perimeter, this gives an average value of u_*. For a two-dimensional fully developed flow, or flow in a wide channel (the aspect ratio, B/h>6 where B is the channel width) h is used in place of the R_h (Muste and Patel 1997, Graf and Altınakar 1998). Yang (2010) investigated the influence of flow geometry on the depth-average shear stress and velocity. Muste and Patel (1997) claimed that this method were of less accuracy because they incorporate errors due to piezometers and flow depth readings. The shear velocity estimated by Eq. (3) is abbreviated as u_{*UN}:

In unsteady flows the u_* becomes $u_* = (ghS_e)^{1/2}$ where S_e is the slope of energy grade line. Saint-Venant equations consist of continuity as given in Eq. (4) and momentum equations. One can derive the latter by equating the momentum on a control volume in conservative form or in non-conservative form as given in Eq. (5a) and Eq. (5b), respectively.

$$\frac{\partial Q}{\partial x} + \frac{\partial A}{\partial t} = 0 \qquad (4)$$

$$\frac{1}{A}\frac{\partial Q}{\partial t} + \frac{1}{A}\frac{\partial}{\partial x}\left(\frac{Q^2}{A}\right) + g\frac{\partial h}{\partial x} - g\left(S_0 - S_e\right) = 0 \qquad (5a)$$

$$\frac{\partial V}{\partial t} + V\frac{\partial V}{\partial x} + g\frac{\partial h}{\partial x} - g\left(S_0 - S_e\right) = 0 \qquad (5b)$$

where A is the cross sectional area, V is velocity and $S_0 = -\partial z/\partial x$. After mathematical manipulations, one can get;

$$u_* = \sqrt{gR_h\left(-\frac{\partial z}{\partial x} - \frac{\partial h}{\partial x} - \frac{V}{g}\frac{\partial V}{\partial x} - \frac{1}{g}\frac{\partial V}{\partial t}\right)} \qquad (6)$$

The shear velocity estimated by Eq. (6) is abbreviated as u_{*SV}:

3. Velocity Data at the Viscous Sub Layer:

The velocity distribution in a cross section of the flow in a channel has risen up attention of many researchers. For smooth walls, the velocity profile in the viscous sublayer is linear and fits to the

equation given below (Lopez and Garcia 1999).

$$u/u_* = z\,u_*/\nu \tag{7}$$

In unsteady flows, the velocity profile at each time instant is examined independently and the u_* is calculated for each profile, so that a time variation of u_* is obtained. Onitsuka and Nezu (1999) revealed that the linear distribution is valid both in rising and falling limbs. The drawback of the method is the limited number of data within this thin layer (Nezu and Nakagawa 1993).

4. Clauser Method (u_{*L}):

Nikuradse (1933) has proposed a logarithmic law to describe the vertical distribution of u. The shear velocity may be obtained from the slope of the best fit line in the inner region where $\chi=z/h<0.2$ (Graf and Altınakar, 1998). When $u_*k_s/\nu < 5$ the flow is assumed to be smooth and the Eq. (8) is valid.

$$\frac{u}{u_*} = \frac{1}{\kappa}\ln\frac{z\,u_*}{\nu} + B_s \tag{8}$$

where k_s is the Nikuradse's equivalent sand roughness, κ is the von Karman constant and equal to 0.40, B_s is the integral constant for smooth boundaries. The rough regime occurs when $u_*k_s/\nu >70$ and the Eq. (9) is valid as,

$$\frac{u}{u_*} = \frac{1}{\kappa}\ln\frac{z+z_0}{k_s} + B_r \tag{9}$$

where z_0 is the reference level, B_r is the integral constant for rough boundaries. In steady flows, the k_s is taken as $3.5d_{84}$ by (Leopold *et al.* 1964), $5d_{50}$ by (Griffiths 1981), d_{65} by (Wiberg and Smith 1987 and Patel and Ranga Raju 1999), $1\sim10d_{50}$ by Liu (2001) for flat sand bed, $2d_{50}$ by Alabi (2006), $2.5d_{50}$ by Beheshti and Ataie-Ashtiani (2010) where d_{65} and d_{84} are particle size at which 65% and 84% by weight of the sample is finer, respectively, d_{50} is the median diameter of the sediment. In unsteady flow experiments Song and Graf (1996) took the roughness height as d_{50}. The reference level for a completely rough bed was taken as $0.033k_s$ by Jan *et al.* (2006) and $-0.25k_s$ by Song and Graf (1996). Muste and Patel (1997) claimed that this method requires 10-12 mean velocity measurements in the near-bed region for a reliable curve fit.

In the outer region, $\chi=z/h>0.2$, the velocity profile deviates from the log law and could be explained by velocity defect law. As given in Eq. (10), Coles (1956) has improved the log law by introducing a wake function $\omega(\Pi)$ given in Eq. (11).

$$\frac{u}{u_*} = \frac{1}{\kappa}\ln\left(\frac{z\,u_*}{\nu},\frac{z}{k_s}\right) + \left(B_s, B_r\right) + \omega(\Pi) \tag{10}$$

$$\omega(\Pi) = \frac{2\Pi}{\kappa}\sin^2\left(\frac{\pi}{2}\frac{z}{h}\right) \tag{11}$$

here, Π is the wake strength parameter.

Brereton *et al.* (1990), Tu and Graf (1992), Tardu *et al.* (1994) and Song and Graf (1996) investigated the velocity profile for unsteady flows and concluded that the logarithmic law is valid in the inner region of open channel flow.

In natural channels the flow is three dimensional due to the presence of secondary currents and the measured maximum velocity occurs below the surface and this is called the velocity dip phenomenon (Guo and Julien 2008 and Guo 2014). A Modified Log-Wake Law (MLWL) is proposed by Guo and Julien (2003) and Guo *et al.* (2005) which is applicable to velocity data measured in both pipe and open channel flow in laboratory and field. Based on the analysis of the Reynolds-averaged Navier–Stokes (RANS) equations and a log-wake modified eddy viscosity distribution, Absi (2011) proposed an ordinary differential equation for velocity distribution to predict the velocity-dip-phenomenon. Bonakdari *et al.* (2008) analyzed Navier–Stokes equations and suggested a new formulation of the vertical velocity profile in the center region of steady fully developed turbulent open-channel flows. Lassabatere *et al.* (2013) integrated the RANS equation by assuming the variations in the transverse direction at the center of the channel could be neglected.

For unsteady flows, Nezu *et al.* (1997) determined that the von Karman constant is not considerably affected from the unsteadiness. The deviation of κ from the value 0.41 depends on the unsteadiness parameter α and concluded that the von Karman constant was not affected from the unsteadiness and can be taken as equal to 0.41 (Onitsuka and Nezu 1999). It is proposed as 0.40 by Song and Graf (1996) and 0.41 by Brereton *et al.* (1990) Tardu *et al.* (1994), Brereton and Mankbadi (1995) and Bares et al. (2008).

The integration constant for smooth boundaries B_s has an average value of 5 (±25%). In unsteady flows, Nezu *et al.* (1997) calculated the B_s as 5.3 in the initial steady part. They find out that the value of B_s decreases in the rising limb of the hydrograph and gets its minimum value just before the peak is reached. The B_s value increases in the falling limb and gets it maximum value in the middle of the falling limb and then again decreases to its original steady value. Akhavan *et al.* (1991) and Nezu *et al.* (1997) obtained similar results. Onitsuka and Nezu (1999) and Nezu and Sanjou (2006) claimed that for hydrographs with small unsteadiness values ($\alpha \approx$ 0.001), the B_s remains nearly constant throughout the hydrograph, but for the ones with higher unsteadiness, ($\alpha \approx$ 0.0063) B_s increases in the rising period and decreases in the falling period.

The integration constant for rough boundaries B_r has an average value of 8.5 (±15%). Song and Graf (1996) revealed that the B_r parameter is equal to 8.5 as an average value. Tu and Graf (1992) calculated B_r in the range of 3.8 - 14.5. Similarly Song (1994) used the velocity data in the inner region to calculate the B_r and concluded that in rising limb B_r has smaller values than the one in the falling limb.

Cellino (1998) used the Clauser method to calculate

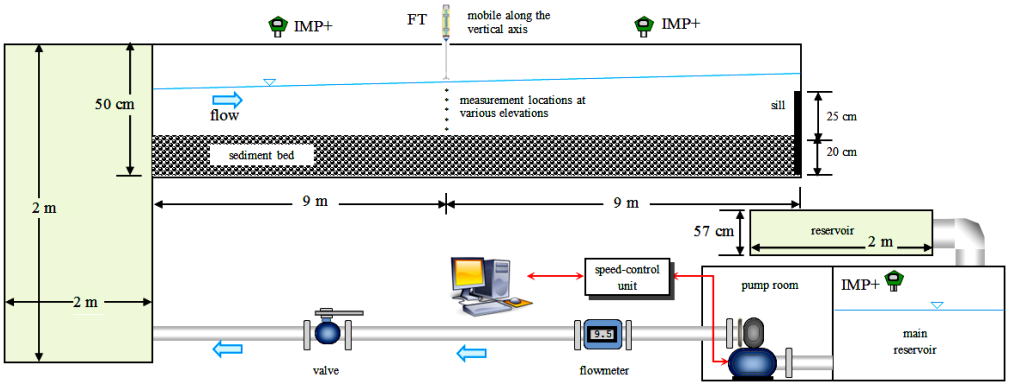

(a)

(b)

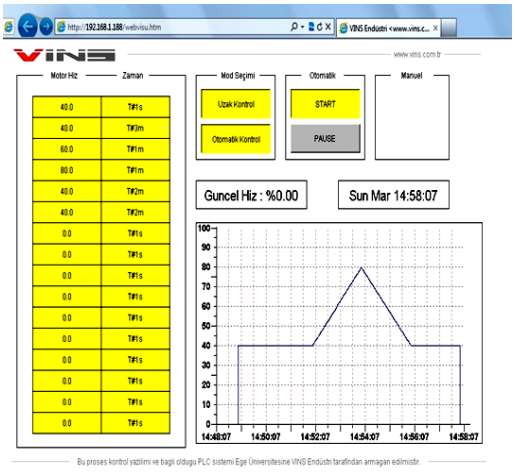

(c)

(d)

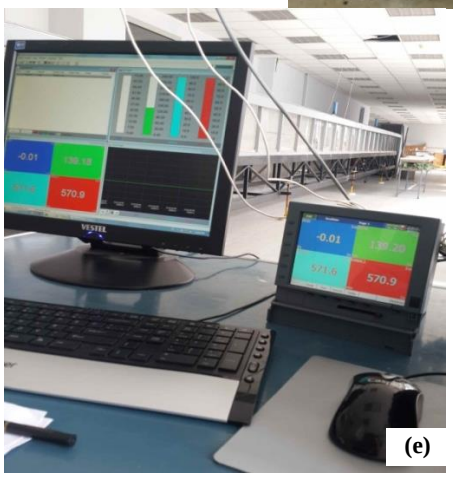

(e)

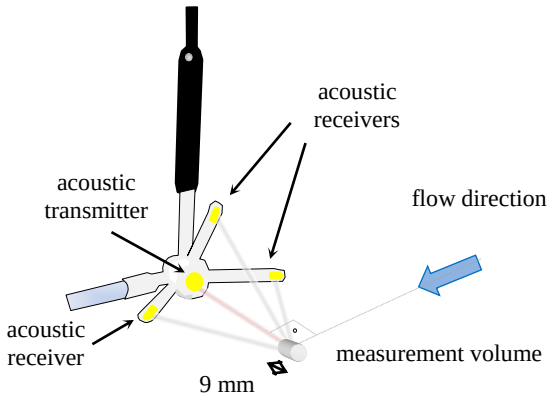

(f)

Fig. 2. (a) Scheme of the experimental setup, (b) PSCU, (c) software of PSCU, (d) flowmeter, (e) flume computer and data logger, (f) Flow Tracker with side-looking sensors (Flow Tracker Users Manuel).

the shear velocity in investigating the effect of suspended sediment flux on the velocity profile in steady flows. The slope of the linear trend line found by least square regression for u versus ln(z) is used to calculate the u_*. The shear velocity estimated by Clauser method is abbreviated as u_{*L}:

For unsteady flows, Song and Graf (1996) find that the log law is valid in the inner region and Coles wake law is valid in the outer region the Nezu and Nakagawa (1991) mentioned that for high Reynolds numbers this deviation from log law is more prominent.

5. Parabolic Law (u_{*P}):

The parabolic law is given by Eq. (12) and applicable for the velocity data in the outer region (Graf and Altınakar 1998).

$$\frac{u_m - u}{u_*} = \lambda \left(1 - \frac{z}{h}\right)^2 \tag{12}$$

where u_m is the maximum velocity, λ is given by the equation below (Afzalimehr *et al.* 2007)

$$\lambda = \frac{2.5}{2\chi(1-\chi)} \tag{13}$$

Taking χ=0.2 will make the λ=7.8. Graf and Altınakar (1998) proposed to take λ as 9.6. Kundu and Gholhal (2012) proposed to take λ as 6.3 proposed by Bazin. The slope of the linear trend line between u and $(1\text{-}z/h)^2$ can be used to calculate the u_*. Afzalimehr et al (2007) used this method successfully for decelerating steady flows. The shear velocity estimated by Eq. (12) is abbreviated as u_{*P}.

6. Average Velocity (u_{*avg}):

The equation given below is used to calculate the shear velocity as u_{*avg}.

$$\frac{V}{u_*} = \frac{1}{\kappa}\ln\left(\frac{R_h}{k_s}\right) + 6.25 \tag{14}$$

Recently, one and two dimensional velocity distribution in open channels is derived by maximizing the Tsallis entropy showing an advantage in capturing low velocities near the channel bed for heavy sediment flows with high entropy value (Cui and Singh 2013, Cui and Singh 2014b). Later Singh *et al.* (2014) derived a function for modelling the flow duration curve. Cui and Singh (2014a,c) computed the sediment discharge and sediment concentration distribution by the same method and revealed that this method has an advantage over other methods for the upper 80% depths.

3. EXPERIMENTAL SET-UP

The experiments were conducted in a rectangular flume of 70 cm width, 18 m length with a bed slope of 0.004 in the Hydraulics Laboratory of Ege University, Department of Civil Engineering. The transparent sides of the flume made from plexiglass were 50 cm high. A tail gate of 25 cm high was located at the end section. The sketch of the experimental setup is given in Fig. 2.a. The bed material used in the flume was composed of a non-uniform sediment mixture with d_{50} = 0.43 mm. Its thickness was 20 cm. The geometric mean diameter was d_g = 0.44 mm and geometric standard deviation was σ_g = 2.27. The uniformity coefficient (Cu = d_{60}/d_{10}) was 3.72. At the first 1.7 m of the flume coarse grains were placed in order to prevent the local scour at the entrance.

The water was circulated continuously. The volume of the water supply reservoir was approximately 47 m^3. The pump used in this study was capable of producing a flow rate up to 100 l/s, and it was connected to a speed-control unit (PSCU) given in Fig. 2.b that can control the flow rate by a program by increasing and/or decreasing the pump speed H_{PSCU} (in percentage of 1450 rpm) at desired time increments. The software window is given in Fig.2.c. An electromagnetic flow meter (Optiflux by Krohne) was mounted on the pipe before the entrance of the channel in order to measure the flow rate with a precision of 0.01 l/s (Fig.2.d). The water depths were measured by means of the level meters (IMP+) with a precision of 0.1 mm which were placed 6 m, 6.75 m, 8.25 m, 9.2 m, 10.75 m and 11.25 m from the upstream end of the flume. The IMP+s and the flow meter are connected to a data logger (by Brainchild) which can record the data instantaneously as given in Fig 2.e.

The ultrasonic instruments have been used in discharge, suspended measurements and pollutant fluxes in open channels and sewers (Abda *et al.* 2008 and Larrarte and Le Barbu 2010). The 3D velocities are measured by such an instrument namely Flow Tracker (FT by Sontek) which is located at 9 m from the entrance of the channel. The acoustic transmitter generates a short pulse of sound with the majority of energy concentrated in a narrow beam which is 6 mm in diameter. The acoustic receivers are mounted on arms from the central probe head. The receivers are sensitive to a narrow beam and are focused on a common volume located a fixed distance which is 10 cm from the probe. The sampling volume is the physical location of the water velocity measurement. It also includes a temperature sensor mounted inside the probe. The temperature data is used to compensate for changes in sound speed. Sound speed is used to convert the Doppler shift to water velocity (Flow Tracker Users Manuel). A scheme of FT with side-looking sensors is presented in Fig. 2.f, for illustrative purposes. The length of the cylindrical measurement volume is 9 mm which is located perpendicular to the flow direction. The volume of the cylindrical shaped remote sensing volume is 0.25 cc. Unlike ADVP (Song and Graf, 1996) and Ultrasonic Velocity Profiler (UVP) (Bares *et al.* 2008), the point velocity measurement devices such as micro-mouline (Tu 1991, Qu 2002), LDA (Nezu *et al.* 1997) and FT, one has to repeat the hydrograph while changing the elevation of the instrument along the flow depth in order to obtain the velocity profile. The instantaneous time series of velocity

components were measured at various elevations.

The sampling frequency of all the instruments (level meters, flow meter and velocity meter) was 1 Hz. All the experiments were recorded by a camera and a chronometer is used in order to check and validate the synchronization of the instruments and the PSCU.

Three different triangular-shaped asymmetrical hydrographs were generated in the flume with same base and peak H_{PSCU} as 35% and 70% but different design rising durations as 180 s, 270 s and 540 s, for Exp1, Exp2 and Exp3, respectively. Their falling duration was 60 s. The flow rate was increased slowly and when the base flow was reached the hydrograph was started. No sediment transport was observed during the base and peak flow conditions.

4. PRELIMINARY RESULTS OF EXPERIMENTS

The velocity readings were taken 9 m from the flume entrance and at different vertical positions from the bed within the flow depth at least 10 points, which some of them were repeated more than twice (Fig. 3). The sampling time for Exp1 is 380 seconds, for Exp2 is 460 seconds and for Exp3 720 seconds for each experiment. The measurements in this experiment were taken in the Cartesian coordinate system x and z. The coordinate x is defined as the distance from the entrance of the flume, y is the transverse distance from the center line which is

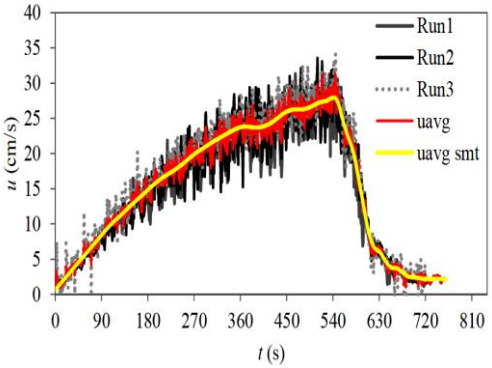

Fig. 3. Variation of velocity with time for repeated runs (Run1, Run2 and Run3), their average and the smoothed value of the average velocity for hydrograph in Exp3.

the line of symmetry of the center line of flume, and z is the vertical distance from the surface of the bed.

The u and w are the instantaneous point velocities in x and z directions can be decomposed into time varying mean point velocities $\overline{u}$ and $\overline{w}$ and their time varying fluctuating components of point velocities u' and w' as $u = \overline{u} + u'$ and $w = \overline{w} + w'$. There are procedures proposed for obtaining the time varying mean for unsteady flows such as Fourier Transform, Wavelet, Moving average etc. (Bombar *et al.* 2010). In this case the moving average algorithm is adopted in which the nth data is equal to the average of previous and proceeding 10 measured velocity data, totally 21 data including itself, as given in Eq. (15). Signal-to-noise ratio (SNR) is the ratio of the received acoustic signal strength to the ambient noise level. It is expressed in logarithmic units as dB (Flow Tracker Users Manuel). The velocity time series were carefully inspected before the analysis and concluded that the minimum SNR never becomes less than 15.

$$\overline{u}_n = \sqrt{\frac{1}{21}\sum_{i=n-10}^{n+10} u_i} \tag{15}$$

There are two main reasons for smoothing the raw velocity time series. The smoothed velocity time series is used only in calculating the partial derivative of cross sectional mean velocity with respect to time $\partial V / \partial t$ in Saint-Venant method. The second reason is to obtain the time that the parameter attains its maximum value accurately. These values are also given in Table 1. In the rest of the calculations, the raw velocity time series is used in the calculations. As an example the velocity time series obtained by three repetitions as Run1, Run2 and Run3 at z=4.5 cm as well as their average u_{avg} and the smoothed average as $u_{avg\ smt}$ for Exp3 are depicted in Fig. 3.

Table 1 Characteristics of the experiments

Parameter	Exp1	Exp2	Exp3
Q_{base} (l/s)	2.06	2.06	2.06
$Q_{FM\ peak}$ (l/s)	38.8	38.4	39.3
ΔQ_{FM} (l/s)	36.7	36.4	37.3
$T_{r\ QFM}$ (s)	187	273	544
$Q_{VM\ peak}$ (l/s)	37.0	37.0	38.9
ΔQ_{VM} (l/s)	34.9	34.9	36.8
$T_{r\ QVM}$ (s)	186	274	539
$Q_{FM\,peak}$-$Q_{VM\,peak}$(%)	4.9	3.8	1.0
h_{base} (cm)	12.16	12.16	12.16
h_{peak} (cm)	20.10	20.57	20.80
Δh (cm)	7.94	8.41	8.64
T_r (s)	194	282	553
T_f (s)	218	230	210
$\Delta T = T_r + T_f$	412	512	763
V_{base} (cm/s)	2.42	2.42	2.42
V_{peak} (cm/s)	25.70	25.90	26.90
ΔV (cm/s)	23.48	23.48	24.48
$V_c = (V_{base}+V_{peak})/2$	14.06	14.16	14.66
$T_{r\,V}$ (s)	186	272	537
F $_{base}$	0.022	0.022	0.022
F $_{peak}$	0.183	0.182	0.188
α	0.003	0.002	0.001

The average velocity at any instant time V is calculated by taking the average of the instantaneous point velocities along the water column. Assuming V as the mean cross sectional velocity, the discharge is obtained as $Q_{VM} = VhB$. The discharge obtained from the electromagnetic flow meter mounted on the pipe is denoted as Q_{FM}. The time variation of Q_{FM} and Q_{VM} are depicted in Fig. 4.

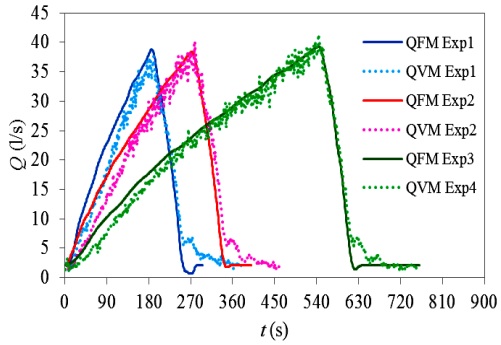

Fig. 4. Time variation of the Q_{FM} and Q_{VM}.

The total volume of water under the hydrograph Exp1 are 5.87 m^3 and 5.55 m^3 (5.4% difference) considering Q_{FM} ($\forall_{FM}$) and Q_{VM} ($\forall_{VM}$), respectively. The volume obtained in the pipe 14.34 m^3 and in the flume is 13.93 m^3 (2.8% difference). The average value for the ratio throughout the experiments is 1.059 for Exp1, 1.043 for Exp2 and 1.030 for Exp3. Therefore the measurements can be considered to be representing the discharge in the flume satisfying the continuity within the experimental system. This shows that the flow rate do not change too much for pipe flow and for open channel flow.

The flow depth variation with dimensionless time (t/T_r) at x= 9 m is given in Fig. 5. At the base flow, before the hydrograph started, the water surface slope was determined by measuring the flow depth at various points and calculated as $\partial h/\partial x_{\text{base}}$ = 0.0033. The variation of the water surface profile is given in Fig. 6.a and Fig. 6.b for Exp1 and Exp3, respectively. The profiles are given at times 0.0, 0.2, 0.4, 0.6, 0.8 and 1.0 times T_r of the rising period. It is observed that the water depth at the downstream never becomes smaller than the upstream water depth for all phases of the hydrograph.

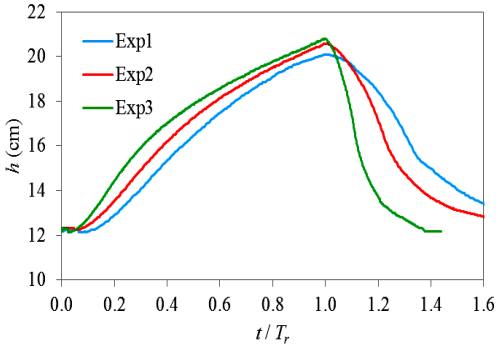

Fig. 5. Variation of flow depth h with t/T_r.

The characteristics of the experiments are given in Table 1. Here F_{base} and F_{peak} are the Froude numbers at base and peak flow conditions, respectively. The subscripts "VM" and "FM" corresponds to the parameter obtained considering Q_{VM} and Q_{FM}, respectively. $T_{r\ V}$ is the rising duration considering the velocity. As seen from the table, all experiments were conducted under subcritical flow conditions.

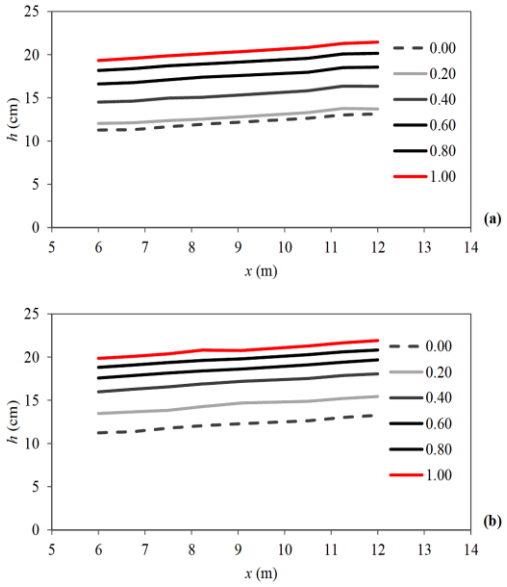

Fig. 6. Water surface slopes at various times for (a) Exp1 and (b) Exp3.

5. ESTIMATION OF SHEAR VELOCITY

The methods given in the introduction part for calculating the shear velocity are adopted for the case in this study. Among them, the momentum equation (u_{*UN}), the Saint-Venant method (u_{*SV}), Clauser Method (u_{*L}) the Parabolic Law (u_{*P}), and (u_{*avg}) are used. The velocity data in the viscous sub-layer could not be measured since the boundary layer thickness 11.6ν/u_* is very small, therefore this method was not used. Also since the total shear stress does not obey the linear distribution any longer in unsteady flows, it is decided not to use the Reynolds Stress graph method. The shear velocities are calculated and discussed below.

5.1. Shear Velocity Calculations

1. The Slope Method, Saint-Venant Equations (u_{*UN} & u_{*SV}):

The velocity measurements were carried out only at one section i.e. 9 m from the channel entrance. Therefore it was not possible to calculate the term $(-V/g)\partial V/\partial x$ in Eq. (6). This term has an order of magnitude 10^{-5} while the S_0 or S_e has an order of 10^{-3} (Graf and Altınakar, 1998). It was assumed that the spatial variation of velocity in the channel is negligible (Powell *et al.* 2001, Hassan *et al*. 2006). Therefore the term $(-V/g)\partial V/\partial x$ is interpreted as $\partial Q/\partial x = 0$ thus the shear velocity becomes,

$$u_* = \sqrt{gR_h\left(S_0 + \frac{\partial h}{\partial x}\left(\frac{1}{g}\frac{V^2}{h} - 1\right) - \frac{1}{g}\frac{\partial V}{\partial t}\right)} \qquad (16)$$

The variation of $\partial h/\partial x$ (V^2/gh-1) term with normalized time t/T_r is given in Fig. 7.

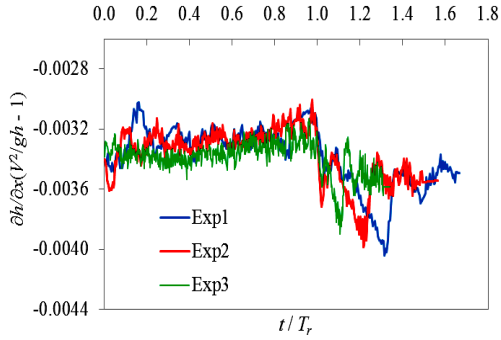

Fig. 7. The variation of $\partial h/\partial x$ (V^2/gh-1) term with normalized time t/T_r.

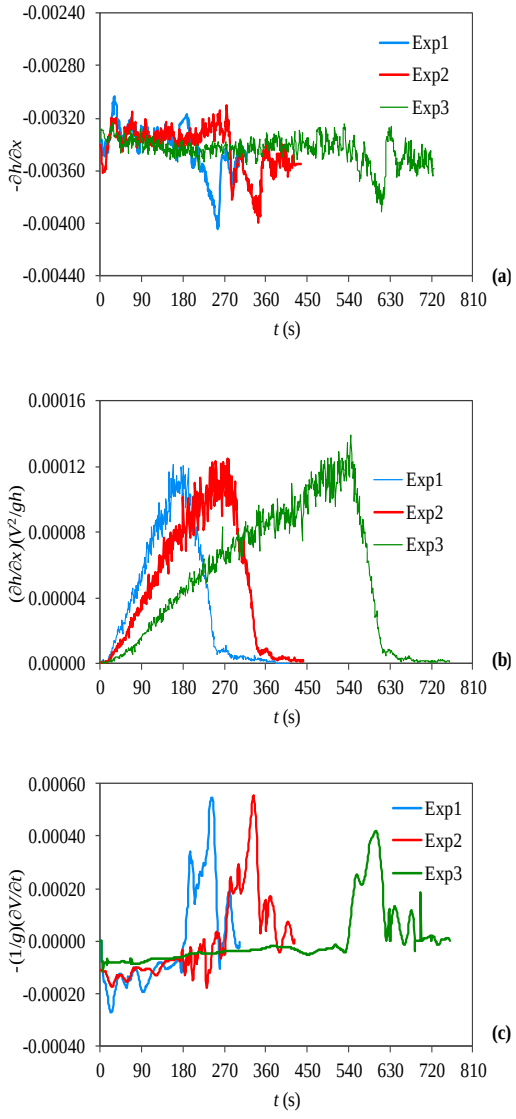

Fig. 8. (a) second, (b) third and (c) fourth terms in Eq. (17) for experiments.

One can rewrite the Eq. (16) as Eq. (17). The time variation of the second, third and fourth terms in the parenthesis of Eq. (17) which are $-\partial h/\partial x$, $(V^2/gh)\partial h/\partial x$ and $(1/g)\partial V/\partial t$, respectively are given in Fig. 8.a, 8.b and 8.c, respectively for the experiments. The minimum value of $\partial h/\partial x$ occurs at 250 s, 340 s and 620 s for Exp1, Exp2 and Exp3, respectively. The spatial-variation of the flow depth depends on the downstream boundary conditions of the flume. It is equal to 0.0034 for the leading and tailing steady flows, i.e. the steady parts preceding and proceeding the hydrograph. When the flow increases, the spatial-variations of the flow depth, h start to decrease till minimum values of 0.004 when the flow reaches its peak value. The spatial-variation of h went back to their steady state after fluctuating around it.

$$u_* = \sqrt{gR_h\left(S_0 - \frac{\partial h}{\partial x} + \frac{1}{g}\frac{V^2}{h}\frac{\partial h}{\partial x} - \frac{1}{g}\frac{\partial V}{\partial t}\right)} \qquad (17)$$

The variation of the second term $(V^2/gh)(\partial h/\partial t)$ with time attains its peak value as 180 s, 270 s and 540 s for the hydrographs Exp1, Exp2 and Exp3, respectively. The third term $-(1/g)(\partial V/\partial t)$ for Exp1 has more fluctuations in the rising limb when compared with those for Exp2 and Exp3. This is attributed again to the wave propagation in the flume. It is seen that the magnitude of the second and third terms are much less than spatial-variations. Obviously the spatial-variations have the dominating roles as mentioned by Qu (2002).

2. Clauser Method (u_{*L}):

In this study the Clauser Method used by Cellino (1998) was adopted and modified for the unsteady flow case. The linear best fit line of u versus $\ln(z)$ was obtained for each velocity profile measured at each sampling time as performed by Qu (2002), Nezu and Sanjou (2006) and Tu (1991). The mean value of the correlation coefficients R^2 for Exp1 was around 0.8 and for Exp2 and Exp3, it is 0.6.

3. Parabolic Law (u_{*P}):

The correlation coefficient R^2 is calculated as 0.6 for Exp1, 0.56 for Exp2 and 0.55 for Exp3, when the best fit line is drawn between u and $(1-z/h)^2$. The λ is taken as 7.8 and the maximum velocity calculated from the u intercept. As depicted in Fig. 9, the u_m obtained from the measured velocity time series is in accord with the calculated one for all experiments.

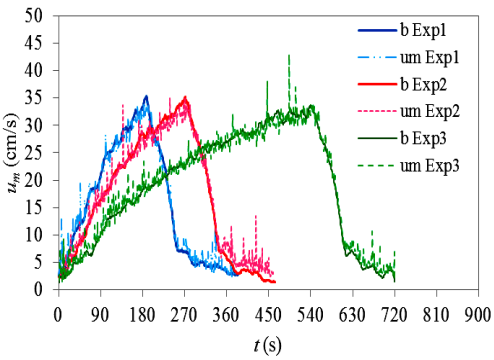

Fig. 9. u_m obtained from the measured velocity and calculated by Eq. (12).

4. Average Velocity (u_{*avg}):

The Eq. (14) is used to find the shear velocity by using the mean average velocity V. The equivalent sand roughness was taken as $k_s = 10\ d_{50}$.

5.2. Comparison of the Results

The time variation of the obtained shear velocities named as u_{*UN}, u_{*SV}, u_{*L}, u_{*P} and u_{*avg} are depicted in Fig. 10.

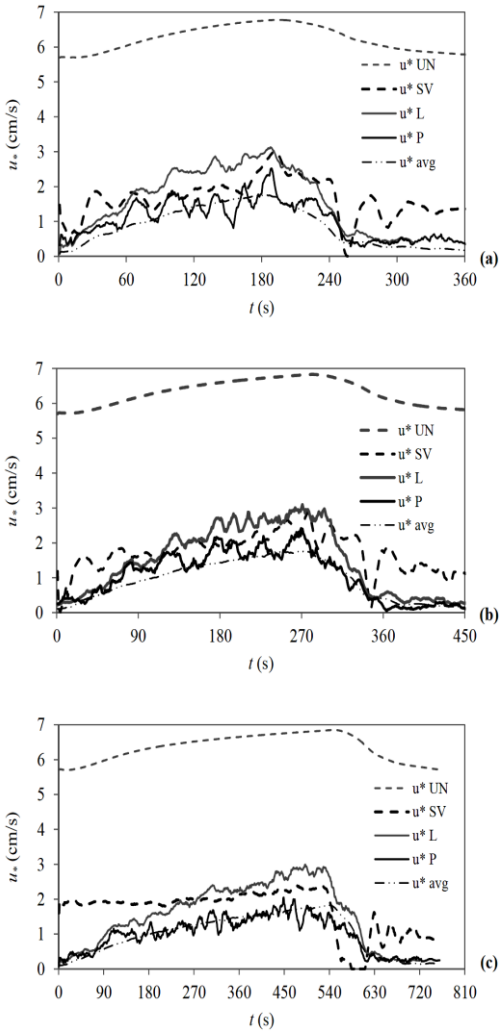

Fig. 10. The variation of the shear velocity u_* with time for (a) Exp1, (b) Exp2 and (c) Exp3.

The percentage deviations from the shear velocity found by Clauser method from the other shear velocities are calculated and the root mean square values are given in Table 2, for the rising, falling and total durations. Kironoto (1993) calculated the shear velocity by the Reynolds stress graph and Clauser Method. He found the greatest deviation from the shear velocity obtained by Clauser method is the one found by energy slope method. The percentage difference was in the range of ±20%. Qu (2002) calculated the shear velocity by Clauser method, slope method and in his conclusions in his study on sediment transport. Qu (2002) found that the shear velocity, u_{*SV} estimated from Saint-Venant equations is smaller than the others. There is no one shear velocity whose root mean square (RMS) value is the lowest for all. Afzalimehr *et al* (2007) also mentioned that the parabolic law is applied when the data are far from the bed so as a reference the shear velocity calculated by the parabolic law is also considered and the deviations found by parabolic law are given in Table 3. Unlike the Clauser method, it is observed that the shear velocity calculated by average velocity equation has particularly the lowest RMS value. The critical shear velocity u_{*UN} was overestimated due to the steady and uniform flow assumption. The u_{*SV} was also overestimated particularly during the first phases of the hydrograph. On the other hand u_{*P} and u_{*avg} coincides well. It is concluded that the shear velocities found by the parabolic law and the average velocity equation can be used interchangeably.

Table 2 Deviation of the shear velocities from the one calculated by Clauser method

		RMS (cm/s)			
		u_{*UN}	u_{*SV}	u_{*P}	u_{*avg}
Exp1	Rising	4.36	0.56	0.81	0.91
	Falling	5.39	0.93	0.49	0.53
	Total	4.90	0.77	0.67	0.74
Exp2	Rising	4.54	0.50	0.58	0.80
	Falling	5.18	0.81	0.68	0.65
	Total	4.72	0.60	0.60	0.76
Exp3	Rising	4.61	0.70	0.79	0.74
	Falling	5.51	1.00	0.36	0.22
	Total	4.84	0.78	0.71	0.66

Table 3 Deviation of the shear velocities from the one calculated by parabolic law

		RMS (cm/s)			
		u_{*UN}	u_{*SV}	u_{*P}	u_{*avg}
Exp1	Rising	5.00	0.55	0.81	0.35
	Falling	5.44	0.87	0.49	0.24
	Total	5.23	0.73	0.67	0.30
Exp2	Rising	5.03	0.60	0.39	0.34
	Falling	5.32	0.88	0.76	0.24
	Total	5.18	0.76	0.60	0.29
Exp3	Rising	5.26	0.92	0.79	0.21
	Falling	5.72	0.77	0.36	0.18
	Total	5.37	0.89	0.71	0.20

5.3. Velocity Profiles

The velocity profile measured and the velocity values obtained by logarithmic and parabolic laws are given in Fig. 11 at t/T_r equal to 0.3, 0.6 and 0.8 for the experiments. Here the solid line represents the best fit line obtained by logarithmic and parabolic laws. Kundu and Ghoshal (2012) also combined the logarithmic law for inner region and the parabolic law for outer region.

6. HYSTERESIS

The variation of the mean point velocities at z=2.5 cm as $u_{2.5}$ and at z=10.5 cm as $u_{10.5}$ are depicted in Fig. 12 with respect to flow depth. The maximum

velocity values are also given in the same figure. As it is expected the maximum velocity values at z=10.5 cm are all greater than the ones corresponding to the velocity values at z=2.5 cm. The ratios are 1.21, 1.18 and 1.13 for Exp1, Exp2 and Exp3, respectively. This reveals that the greater the unsteadiness the higher the maximum point velocity occurs close to the surface than close to the bottom.

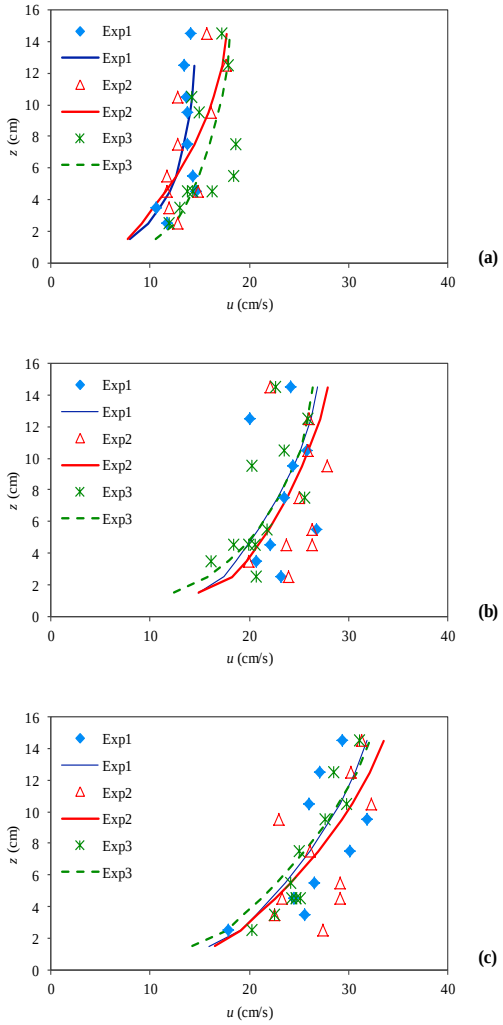

Fig. 11. Velocity profiles for the experiments at for (a) t/T_r = 0.3, (b) t/T_r = 0.6 and (c) t/T_r = 0.8, here the solid line represents the best fit line.

The clock-wise hysteresis is observed for both hydrographs given in Fig 12. The rising and falling limbs are close to each other for Exp3 in which the unsteadiness is small whereas for Exp1, the limbs become further apart. This distance between the limbs depends on the unsteadiness of the hydrograph as mentioned by Graf and Altınakar (1998).

A hysteresis intensity parameter η is proposed as given in equation below in order to calculate how far the limbs from each other. The area between the limbs is normalized by the unit discharge difference of corresponding to the peak and base values, q_{peak} and q_{base}, respectively.

$$\eta = \frac{\sum_{i=1}^{n-2} (h_{i+2} - h_i)\, u_{i+1} / 2}{q_{peak} - q_{base}} \tag{18}$$

It is revealed that the hysteresis intensity parameter η increases with flow depth, in other words the more you are close to the surface the hysteresis is felt more.

It may also be concluded that the constant of the power trend line curve drawn for Exp1 is greater than the one obtained for Exp2 which is also greater than Exp3. This means the more the unsteady the hydrograph the more the hysteresis η.

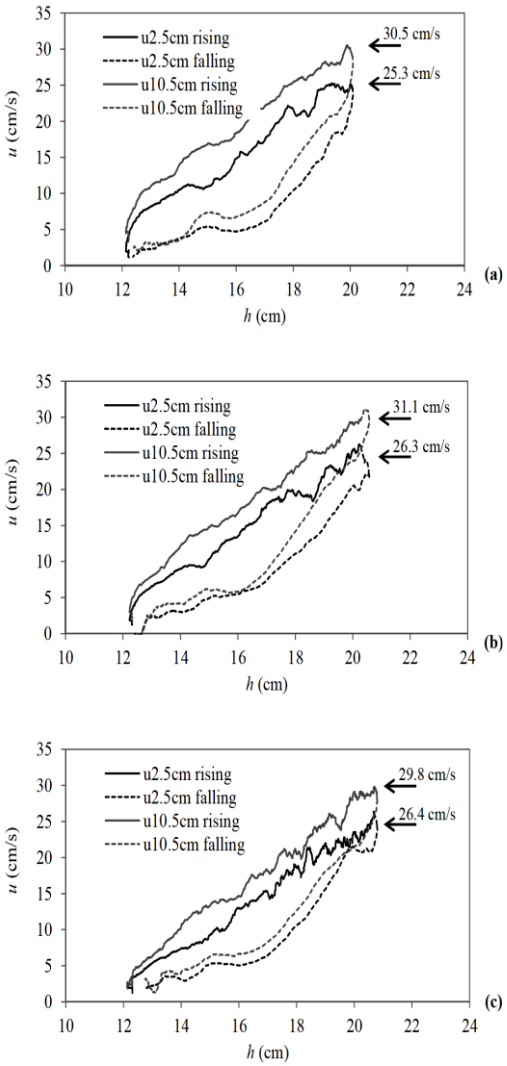

Fig. 12. Variation of *u* with *h* (a) Exp1, (b) Exp2 and (c) Exp3.

The variation of hysteresis intensity parameter η with normalized elevation as z/h_{base}, is depicted in Fig. 13. One can observe that there is a relation between these two dimensionless parameters which are given in Eq. (19.a), Eq. (19.b) and Eq. (19.c) below for Exp1, Exp2 and for Exp3, respectively.

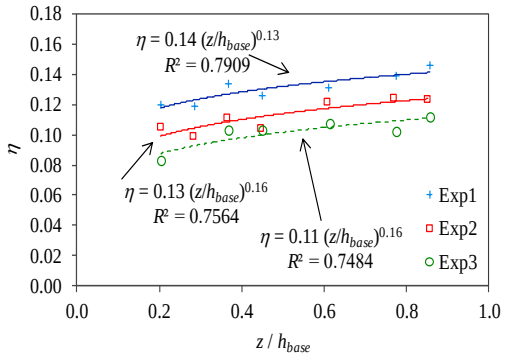

Fig. 13. The variation of η with z/h_{base}.

$$\eta = 0.14\left(\frac{z}{h_{base}}\right)^{0.13} \quad (19.a)$$

$$\eta = 0.13\left(\frac{z}{h_{base}}\right)^{0.16} \quad (19.b)$$

$$\eta = 0.11\left(\frac{z}{h_{base}}\right)^{0.16} \quad (19.c)$$

The variation of cross sectional mean velocity V and flow depth h is given in Fig. 14. It is observed that when the unsteadiness is less as for Exp3, the rising and falling limbs are close to each other, whereas for Exp1, the limbs become further apart. When the mean average velocity V_{i+1} is inserted for u_{i+1} in Eq. (18), the hysteresis intensity parameter is calculated as 0.12, 0.11 and 0.09 for Exp1, Exp2 and Exp3, respectively.

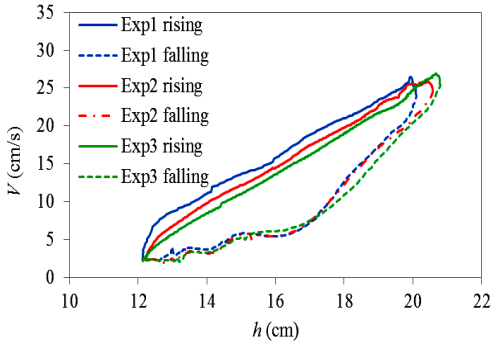

Fig. 14. The variation of velocity V with h.

7. CONCLUSION

The shear velocity is an important parameter in characterizing the shear at the boundary and there exist methods to estimate the shear velocity in steady flows. These methods are listed as the use of the Saint-Venant equations u_{*SV}, use of the procedure given by Clauser Method u_{*L}, use of the parabolic law u_{*P}, use of the momentum equation assuming the slope of energy grade line is equal to bed slope u_{*UN} and use of the average velocity equation u_{*avg}. The methods which are used to calculate the shear velocity in steady flows were tested under unsteady flow conditions for three asymmetrical triangular-shaped hydrographs.

The stream-wise and vertical components of velocity time series and the velocity profiles were obtained by means of an acoustic Doppler velocity meter. The instantaneous velocity time series were obtained at various vertical elevations and the moving average algorithm is adopted to obtain the time varying mean velocity. The variation of flow depth at various locations along the flume was used to calculate the water surface and energy slope variation. It is observed that the water depth at the downstream never becomes smaller than the upstream water depth which means a positive water surface slope throughout the flume for all phases of the hydrograph. Assuming the spatial variation of velocity in the channel is negligible, the Eq. (17) is obtained by which the u_{*SV} can be calculated. It is seen that the magnitude of the second $((V^2/gh)\partial h/\partial x)$ and third $((1/g)\partial V/\partial t)$ terms are much less than spatial-variations. Obviously the spatial-variations $(-\partial h/\partial x)$ have the dominating roles. The momentum equation assuming the flow is uniform was used to calculate the shear velocity u_{*UN}.

The shear velocity was also calculated as u_{*L} by using the Clauser method. The shear velocity calculated by using the parabolic law as u_{*L} and it is observed that the maximum velocity um obtained from the measured velocity time series is in accord with the calculated one. The well-known average velocity equation was used to obtain the shear velocity as u_{*avg}.

Among the methods, u_{*UN} and particularly during the first phases of the hydrograph u_{*SV} were overestimated. On the other hand u_{*P} and u_{*avg} coincides well. It is concluded that the shear velocities found by the parabolic law and the average velocity equation can be used interchangeably.

The logarithmic law for inner region and the parabolic law for outer region combined in order to obtain the mean velocity profiles. Furthermore the hysteresis was investigated and a hysteresis intensity parameter is proposed in order to see the depth variation of hysteretic behavior at point velocity. It is revealed that the hysteresis intensity parameter η increases with flow depth, in other words the more you are close to the surface the hysteresis is felt more. The hysteresis parameter was adapted to the variation of cross-sectional mean velocity and flow depth. It is revealed that the more the unsteady the hydrograph the more the hysteresis both in terms of point velocity and cross-sectional mean velocity.

ACKNOWLEDGEMENTS

The author would like to express her gratitude to Assoc. Prof. Şebnem ELÇİ for supplying the ultrasonic velocity meter used during the execution of the experiments.

REFERENCES

Abda, F., A. Azbaid, D. Ensminger, S. Fischer, P. François, P. Schmitt and A. Pallarés (2008) Ultrasonic device for real-time sewage velocity and suspended particles concentration measurements. *11th International Conference on Urban Drainage*, ISUD, Edinburgh, Scotland, UK.

Absi, R. (2011) An ordinary differential equation for velocity distribution and dip-phenomenon in open channel flows. *Journal of Hydraulic Research* 49(1), 82–89.

Afzalimehr, H., S. Dey and P. Rasoulianfar (2007). Influence of decelerating flow on incipient motion of gravel-bed stream. *Sadhana* 32(5), 545-559.

Akhavan, R., R. D. Kamm and A. H. Shapiro (1991). An investigation of transition to turbulence in bounded oscillatory stokes flows. *Journal of Fluid Mechanics* 225, 395-422.

Alabi, P. D. (2006). *Time development of local scour at a brıdge pıer fıtted wıth a collar*, M.Sc. Thesis, University of Saskatchewan, Canada.

Bagherimiyab, F. (2012). *Sediment suspension dynamics in turbulent unsteady, depth-varying open-channel flow over a gravel bed*. PhD Thesis No: 5168, Ecole Polytechnique Fédérale (EPFL), Lausanne, Switzerland.

Bares, V., J. Jirak and J. Pollert (2008). Spatial and temporal variation of turbulence characterisitcs in combined sewer flow. *Flow Measurement and Instrumentation* 19(3-4), 145-154.

Beheshti, A. A. and B. Ataie-Ashtiani (2010). Experimental study of three-dimensional flow field around a complex bridge pier. *Journal of Engineering Mechanics* 136(2), 143-154.

Bombar, G. (2014). Velocity time series obtained around a bridge pier during a scour hole development. Proceedings of 3rd IAHR Europe Congress, Porto, Portugal.

Bombar, G., M. Ş. Güney, G. Tayfur and Ş. Elçi (2010). Calculation of the time-varying mean velocity by different methods and determination of the turbulence intensities. *Scientific Research and Essays* 5(6), 572-581.

Bombar, G., Ş. Elçi, G. Tayfur, M. Ş. Güney and A. Bor (2011). Experimental and numerical investigation of bedload transport under unsteady flows. *Journal of Hydraulic Engineering* 137(20), 1276-1282.

Bonakdari, H., F. Larrarte, L. Lassabatere and C. Joannis (2008). Turbulent velocity profile in fully-developed open channel flows. *Environmental Fluid Mechanics* 8(1), 1–17.

Bose, S. K. and S. Dey (2012). Turbulent unsteady flow profiles over an adverse slope, *Acta Geophysica* 61(1), 84-97.

Brereton, G. J. and R. R. Mankbadi (1995). Review of recent advances in the study of unsteady turbulent internal flows. *Applied Mech. Rev*. 48(4), 189-212.

Brereton, G. J., W. C. Reynolds and R. Jayaraman (1990). Response of a turbulent boundary layer to sinusoidal free-stream unsteadiness. *Journal of Fluid Mechanics* 221, 131-159.

Cardoso, A. H., W. H. Graf and G. Gust (1989). Uniform flow in a smooth open channel. *Journal of Hydraulic Research* 27(5), 603-616.

Cellino, M. (1998). *Experimental study of suspension flow in open channels*, PhD Thesis, No. 1824, Ecole Polytechnique Fédérale (EPFL), Lausanne, Switzerland.

Coles, D. (1956). The law of the wake in the turbulent boundary layer, *Journal of Fluid Mechanics* 1(2), 191-226.

Cui, H. and V. P. Singh (2013) Two-dimensional velocity distribution in open channels using Tsallis Entropy. *Journal of Hydraulic Engineering* 18(3), 331–339.

Cui, H. and V. P. Singh (2014) Computation of suspended sediment discharge in open channels by combining Tsallis Entropy-based methods and emprical formulas. *Journal of Hydraulic Engineering* 19(1), 18–25.

Cui, H. and V. P. Singh (2014) One-dimensional velocity distribution in open channels using Tsallis Entropy. *Journal of Hydraulic Engineering* 19(2), 290–298.

Cui, H. and V. P. Singh (2014) Suspended sediment concentration in open channels using Tsallis Entropy. *Journal of Hydraulic Engineering* 19(5), 966–977.

Debnath, R., A. Mandal, S. Majumder, S. Bhattacharjee and D. Roy (2015). Numerical analysis of turbulent fluid flow and heat transfer in a rectangular elbow. *Journal of Applied Fluid Mechanics* 8(2), 231–241.

FlowTracker Handheld ADV User's Manual Firmware Version 3.1 SonTek/YSI, Inc., 2006.

Genç, O., M. Ardıçlıoğlu and N. Ağıralioğlu (2015). Calculation of mean velocity and discharge using water surface velocity in small streams. *Flow Measurement and Instrumentation*, online publication date: 1-Mar-2015.

Graf, W. H. and M. S. Altınakar (1998). *Fluvial Hydraulics*, John Wiley & Sons Inc.

Griffiths, G. A. (1981). Flow resistance in coarse gravel bed rivers. *Journal of the Hydraulics Division* 107(7), 899-918.

Güney, M. Ş., G. Bombar and A. Ö. Aksoy (2013). Effect of coarse surface development on the bed load transport of bimodal sediment under unsteady flow conditions. *Journal of Hydraulic Engineering* 139(1), 12–21.

Guo, J. (2014). Modified log-wake-law for smooth rectangular open channel flow. *Journal of Hydraulic Research* 52(1), 121–128.

Guo, J. and P. Y. Julien (2003). Modified log-wake law for turbulent flows in smooth pipes. *Journal of Hydraulic Research* 41(5), 493–501.

Guo, J. and P. Y. Julien (2008). Application of the modified log-wake law in open-channels. *Journal of Applied Fluid Mechanics* 1(2), 17–23.

Guo, J., P. Y. Julien and R. N. Meroney (2005). Modified log-wake law for zero-pressure-gradient turbulent boundary layers. *Journal of Hydraulic Research* 43(4), 421–430.

Hassan, M. A., R. Egozi and G. Parker (2006). Experiments on the effect of hydrograph characteristics on vertical grain sorting in gravel bed rivers. *Water Resources Research* (42), 1-15.

Jan, C. D., J. S. Wang and T. H. Chen (2006). Discussion of Simulation of flow and mass dispersion in meandering channel. *Journal of Hydraulic Engineering* 132(3), 339-342.

Jensen, B., B. M. Sumer and J. Fredsoe (1989). Turbulent oscillatory boundary layers at high Reynolds numbers. *Journal of Fluid Mechanics* 206, 265-297.

Kabiri-Samani, A., F. Farshi and M. R. Chamani (2013). Boundary shear stress in smooth trapezoidal open channel flows. *Journal of Hydraulic Engineering* 139(2), 205–212.

Kırkgöz, S. (1989). Turbulent velocity profiles for smooth and rough open channel flow. *Journal of Hydraulic Engineering* 115(11), 1543-1561.

Kırkgöz, S. and M. Ardıçlıoğlu (1997). Velocity profiles of developing and developed open channel flow. *Journal of Hydraulic Engineering* 123(12), 1099–1105.

Kironoto, B. A. (1993). *Turbulence characteristics of uniform and non-uniform, rough open-channel flow*. Ph.D.Thesis, No 1094, Ecole Polytechnique Fédérale (EPFL), Lausanne, Switzerland.

Kumar, P., A. Mishra, N. S. Raghuwanshi and R. Singh (2002). Application of unsteady flow hydraulic-model to a large and complex irrigation system. *Agricultural Water Management* 54, 49-66.

Kundu, S, and K. Ghoshal (2012). Velocity distribution in open channels: combination of log-law and parabolic-law. *World Academy of Science, Engineering and Technology* 68, 2151-2158.

Larrarte, F. and E. Le Barbu (2010). Acoustic profilers and pollutant flux measurements in urban hydrology *NOVATECH Session 2.4*.

Lassabatere, L., J. Pu, H. Bonakdari, C. Joannis and F. Larrarte (2013). Velocity distribution in open channel flows: analytical approach for the outer region. *Journal of Hydraulic Engineering* 139(1), 37–43.

Leopold, L. B., M. G. Wolman and P. Miller (1964). *Fluvial Processes in Geomorphology*, W.H. Freeman and Company 522.

Lhermitte, R. and U. Lemmin (1994). Open-channel flow and turbulent measurement by high-resolution Doppler sonar. J*ournal Atmos. Oceanic Technol*. 11(5), 1295-1308

Liu, Z. (2001). *Sediement transport*, Laboratoriet for Hydraulik og Havnebygning, Instituttet for Vand, Jord og Miljøteknik, Aalborg Universitet.

Lopez, F. and M. H. Garcia (1999). Wall similarity in turbulent open-channel flow. *Journal of Hydraulic Engineering* 125(7), 789-796.

Meselhe, E. A. and F. M. Holly (1993). Simulation of unsteady flow in irrigation canals with dry bed. *Journal of Hydraulic Engineering* 119(9), 1021-1039.

Muste, M. and V. C. Patel (1997). Velocity profiles for particles and liquid in open-channel flow with suspended solids. *Journal of Hydraulic Engineering* 123(9), 742-751.

Nezu, I. (2005). Open-channel flow turbulence and its research prospect in the 21st century. *Journal of Hydraulic Engineering* 131(4), 229-246.

Nezu, I. and H. Nakagawa (1993). *Turbulence in open-channel flows*, IAHR Monograph Series, A. A. Balkema Publishers, Rotterdam, The Netherlands

Nezu, I. and M. Sanjou (2006). Numerical calculation of turbulence structure in depth-varying unsteady open-channel flows. *Journal of Hydraulic Engineering* 132(7), 681-695.

Nezu, I. and W. Rodi (1986). Open channel flow measurements with a laser Doppler anemometer. *Journal of Hydraulic Engineering* 112(5), 335-355.

Nezu, I., A. Kadota and H. Nakagawa (1997). Turbulent structure in unsteady depth-varying open-channel flows. *Journal of Hydraulic Engineering* 123(9), 752–763.

Nezu, I., and H. Nakagawa (1991). Turbulent structures over dunes and its role on suspended sediments in steady and unsteady open-channel flows. *Proc. of Int. Symp. on Transport of Suspended Sediments and its Mathematical Modeling*, IAHR, Firenze 165-189.

Nikuradse, J. (1933). *Laws of flow in rough pipes*, Translation in National Advisory Committee for aeronautics, technical memorandum 1292, NACA, Washington 1950, 62.

Onitsuka, K. and I. Nezu (1999). Effect of unsteadiness on von Karman constant in

unsteady open-channel flows. D1-Turbulent Channel Flows with Macro Roughness Vegetation. 28th Congress of IAHR, Graz, Austria, Conf. Proceedings.

Patel, P. L. and K. G. Ranga Raju (1999). Critical tractive stress of nonuniform sediments. *Journal of Hydraulic Research* 37(1), 39–58.

Powell, D. M., I. Reid and J. B. Laronne (2001). Evolution of bed load grain size distribution with increasing flow strength and the effect of flow duration on the caliber of bed load sediment yield in ephemeral gravel bed rivers. *Water Resources Research* 37(5), 1463-1474.

Qu, Z. (2002). *Unsteady open-channel flow over a mobile bed*. Ph.D. Thesis. No 2688, Ecole Polytechnique Fédérale (EPFL), Lausanne, Switzerland.

Rowınski, P. M., W. Czernuszenko and J. M. Pretre (2000). Time-dependent shear velocities in channel routing. *Hydrological Sciences* 45(6), 881-895.

Shah S. A., A. C. Orifici and J. H. Watmuff (2015). Water impact of rigid wedges in two-dimensonal fluid flow. *Journal of Applied Fluid Mechanics* 8(2), 329-338.

Singh V. P., A. Byrd and H. Cui (2014). Flow duration curve using entrophy theory. *Journal of Hydraulic Engineering* 19(7), 1340-1348.

Song, C. G., I. W. Seo and Y. D. Kim (2012). Analysis of secondary current effect in the modeling of shallow flow in open channels. *Advances in Water Resources* 41, 29-48.

Song, T. (1994). *Velocity and turbulence distribution in non-uniform and unsteady openchannel flow*. Ph.D. Thesis, No. 1324, Ecole Polytechnique Fédérale (EPFL), Lausanne, Switzerland.

Song, T. and W. H. Graf (1996). Velocity and turbulence distribution in unsteady open channel flows. *Journal of Hydraulic Engineering* 122(3), 141-154.

Tardu, S. F, G. Binder and R. F. Blackwelder. (1994). Turbulent channel flow with large-amplitude velocity oscillations. *Journal of Fluid Mechanics* 267, 109-151.

Tu, H. (1991). Velocity distribution in unsteady flow over gravel beds. Ph.D. Thesis, No 911, Ecole Polytechnique Fédérale (EPFL), Lausanne, Switzerland.

Tu, H. and W. H. Graf (1992). *Velocity distribution in unsteady open channel flow over gravel beds*. *Journal of Hydroscience and Hydraulic Engineering* 10(1), 11-25.

Walker, W. R. and A. S. Humpherys (1983). Kinematic-wave furrow irrigation model. *Journal of Drainage and Irrigation Engineering* 109(4), 377–392.

Wiberg, P. L. and J. D. Smith (1987). Calculations of the critical shear stress for motion of uniform and heterogeneous sediments. *Water Resouces Research* 23(8), 1471–1480.

Yang, S. Q. (2010). Depth-averaged shear stress and velocity in open-channel flows. *Journal of Hydraulic Engineering* 136(11), 952–958.

Zhang, S., J. G. Duan, T. S. Strelkoff and E. Bautista (2012). Simulation of Unsteady Flow and Soil Erosion in Irrigation Furrows. *Journal of Irrigation and Drainage Engineering* 138(4), 294–303.